PROCEEDINGS OF SPIE

SPIEDigitalLibrary.org/conference-proceedings-of-spie

Algorithmic improvements and consistency checks of the NOAA global gridded super-collated SSTs from low Earth orbiting satellites (L3S-LEO)

Olafur Jonasson, Irina Gladkova, Alexander Ignatov, Yury Kihai

Olafur Jonasson, Irina Gladkova, Alexander Ignatov, Yury Kihai, "Algorithmic improvements and consistency checks of the NOAA global gridded super-collated SSTs from low Earth orbiting satellites (L3S-LEO)," Proc. SPIE 11752, Ocean Sensing and Monitoring XIII, 1175202 (25 May 2021); doi: 10.1117/12.2585819

SPIE.

Event: SPIE Defense + Commercial Sensing, 2021, Online Only

Algorithmic Improvements and Consistency Checks of the NOAA Global Gridded Super-Collated SSTs from Low Earth Orbiting Satellites (L3S-LEO)

Olafur Jonasson[1,2], Irina Gladkova[1,2,3], Alexander Ignatov[1], Yury Kihai[1,2]

[1]STAR, NOAA Center for Weather and Climate Prediction (NCWCP), USA

[2]Global Science and Technology, Inc., USA

[3]City College of New York, USA

Abstract

NOAA provides sea surface temperature (SST) products from multiple Earth observing satellites in low Earth orbits (LEO) using its Advanced Clear-Sky Processor for Ocean (ACSPO) system. Historically, ACSPO SST products from individual LEO platforms have been provided as 10-minute granules (144/day) in L2P (swath) and 0.02° L3U (gridded uncollated) formats. With the large, and increasing number of LEO sensors currently in orbit (two VIIRSs onboard NPP/N20, three AVHRRs onboard METOP-A/B/C and two MODISs onboard Aqua/Terra) and soon to be launched (N21/VIIRS and Metop-Second Generation METImage), the data volumes and number of files has grown dramatically and is now challenging to manage by an average user. Moreover, data from different sensors and overpasses may not be fully consistent. In response to multiple users' requests, the NOAA SST team has developed the 0.02° gridded super-collated (L3S) line of LEO SST products, which collate L3U data from individual sensors into a multi-sensor products with higher information density, lower data volume consistent datasets. The L3S-LEO line comprises two products: from the afternoon ('PM') orbits (currently, two VIIRSs onboard NPP and N20) and from the mid-morning ('AM') orbits (currently, three AVHRR FRACs onboard Metop-A/B/C). Both products are reported twice daily, one nighttime and one daytime file, resulting in four files every 24 hours. The data are validated in the NOAA SST Quality Monitor (SQUAM) online system, and distributed to users via the CoastWatch service, in near real time. This work describes recent L3S-LEO algorithm developments, aimed at the reduced impact of cloud leakages from individual sensor L3U data, and improved SST imagery. We also present initial checks of the diurnal cycle in the L3S-LEO vs. GEO SST from the Advanced Baseline Imager (ABI) flown onboard GOES-16, and find the two datasets largely consistent.

1. Introduction

With the goal of reconciling SST data products from various low Earth orbit (LEO) satellites and overpasses, and reducing data volumes, to provide more data dense, consistent higher quality SST products, the NOAA STAR SST team has developed a new family of 0.02° gridded super-collated L3S-LEO SST products. We follow the Group for High-Resolution SST (GHRSST) naming convention [1], where the uncollated gridded products are referred to as L3U [2], the collated SST products containing multiple overpasses from a single satellite as L3C, and products combining data from multiple satellites and overpasses as super-collated (L3S). The new L3S-LEO family, introduced in ACSPO version V2.80, comprises two product lines: L3S-PM (from the afternoon, PM satellites with local equator crossing time, LEXT~1:30am/pm) and L3S-AM from the mid-morning, AM satellites (with LEXT~9:30am/pm) ([3], [4]). The PM line is currently produced from two VIIRSs flown onboard NPP and N20, and will include future satellites in the JPSS series. The L3S-AM line is currently produced from the three AVHRR FRAC sensors flown onboard Metop First Generation (FG) series of satellites (Metop-A/B/C). The AM line will also include future satellites from the Metop second generation (Metop-SG) series, which will carry the new METImage sensor. We are also investigating the possibility of adding Terra (launched in Dec'1999) and Aqua (launched in May'2002) MODISs to the AM and PM lines, respectively, to extend the high resolution L3S-LEO PM time series beyond earliest available ACSPO NPP SST data (Feb'2012) [5] and the AM time series before first available ACSPO SST data from Metop-A (Dec'2006) [6].

The PM and AM lines of L3S-LEO products are in turn split into daytime (solar zenith angle ≤ 90°) and night-time (solar zenith angle > 90°) files, resulting in four files per day, hereafter referred to as PM-N, PM-D, AM-N and AM-D, where the N and D suffixes denote nighttime and daytime, respectively. Figure 1 shows the histograms of the local solar observation

Ocean Sensing and Monitoring XIII, edited by Weilin "Will" Hou, Proc. of SPIE Vol. 11752,
1175202 · © 2021 SPIE · CCC code: 0277-786X/21/$21 · doi: 10.1117/12.2585819

times in the four files, demonstrating that the L3S-LEO family may provide coverage of the diurnal cycle at up to four points in time, with an approximate separation of 4 or 8 hours. The potential to capture the diurnal cycle is the main premise for having four L3S-LEO files a day, rather than two or even one. In section 3 we demonstrate the capability of the L3S-LEO to resolve the diurnal cycle and quantify the strength of the diurnal cycle. Another justification for keeping the products separate is that movement of oceanic features over the course of a day can be significant compared to the ACSPO L3S-LEO 0.02° resolution, blurring fine oceanic features. Some NOAA users of ACSPO L3S-LEO have expressed interest in further aggregation of the four data files into one single L3S-daily file. Note that although such aggregation will degrade temporal and spatial feature resolution, it may still be superior to the available gap-free L4 products, and acceptable for some users.

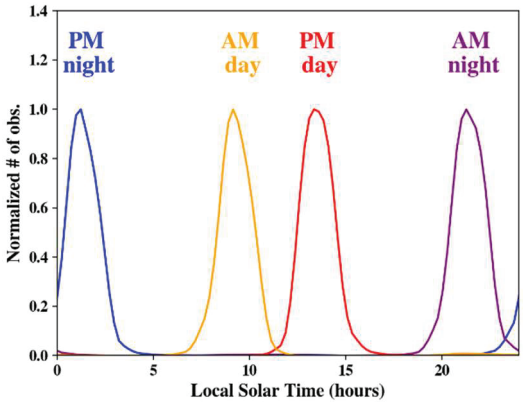

Figure 1. Normalized number of observations in the PM/AM night/daytime L3S-LEO files as a function of local solar time. Data source is aggregated ACSPO L3S-LEO SST data from Jan' 2020.

The ACSPO super-collation algorithm is described in detail in Ref. [4] and only a brief overview will be provided here, highlighting recent updates, to mitigate residual cloud leakages as well as discontinuities in the imagery. The super-collation algorithm comprises four major steps:

1. Create an initial L3S reference SST using all ACSPO L3U data within the collation window (24 hours).
2. Use the L3S reference to mitigate biases between consecutive overpasses, present due to different viewing conditions and acquisition times. The inter-overpass bias mitigation (referred to below as debiasing or normalization) is performed carefully, to preserve features by allowing small spatial scale deviation from the L3S reference, while eliminating large scale regional biases present between consecutive overpasses. For more details on ACSPO L3S-LEO debiasing scheme, we refer the reader to Refs. [3] and [4].
3. L3S SST is computed in every L3 grid from normalized/debiased L3U data using an adaptive weighting procedure which preserves spatial continuity, reduces noise, and mitigates residual cloud leakages which may be present in individual sensor L3U data [4].
4. Steps 2-3 are iterated using the L3S SST from previous iteration as L3S reference.

The major improvement compared to previous work [4] is two-fold. In previous work, the initial L3S reference SST in step 1 was a composite, using the lowest satellite view zenith angle (VZA) measurement available in each L3U 0.02° pixel. The premise for this choice was that measurements taken at low VZAs, are typically more accurate due to the shorter atmospheric path between ocean and sensor. However, routine quality control in the ARMS online system [7] revealed that this approach may lead to propagation of cloud leakages to the final L3S product, if the lowest VZA overpass contained large scale (more than a few pixels) cloud leakages, which typically occur at cloud boundaries. This was the case even when cloud-free measurements were available from other overpasses with measurements made at higher VZAs. Section 2 describes an improved scheme for calculating the initial L3S reference, where input L3U data are weighted based on both VZA and local clear-sky ratio (LCR). The idea is that low VZA measurements are still given higher weight, but pixels near cloud boundaries are assigned lower weight than pixels from a large contiguous clear-sky patches of the ocean. The second improvement is that the generation of the L3S reference is now iterative, where steps 2-3 are repeated three times, using the L3S SST from previous iteration's step 3 instead of the VZA/LCR weighted average in step 1. In each iteration, the debiasing/normalization of input L3U SST to the L3S reference becomes more aggressive (but still allowing for shorter scale deviations from the L3S reference), finally converging to the L3S SST product. This iterative debiasing/normalization scheme was suggested in our previous publication [4], but only now implemented. In section 2 we describe both algorithm changes in detail and provide examples of the effect of these changes on the final L3S-LEO SST product.

ACSPO L3S-LEO SST near-real-time (NRT) products are currently produced in a best effort mode at NOAA STAR with a typical latency of 3-6 hours and made publicly available via the NOAA CoastWatch service [8]. Pending completion of the historical reprocessing (Reanalysis, RAN), 'science quality' SST data will be made available, with a ~8 weeks latency. The PM and AM RAN data will extend back to the first available NPP (Feb'2012) and Metop-A (Dec'2006) data, respectively. Both NRT and RAN ACSPO L3S-LEO data are monitored in the NOAA SQUAM [9] and ARMS [7] online systems. The difference between RAN and NRT data are the following:

1. In NRT processing, ACSPO uses atmospheric data (wind speed as well as profiles of atmospheric temperature and water vapor as input into the Community Radiative Transfer Model, CRTM [10], [11]) from the NOAA Global Forecast System (GFS) [12]. In RAN, data of the Modern-Era Retrospective analysis for Research and Applications (MERRA) [13] produced by NASA are used. MERRA data are released one month at a time, with a latency of approximately 20 days (for example 1-31 January data is available around 20 February).
2. For both NRT and RAN, ACSPO uses the CMC L4 analysis foundation SST product [14] as a first guess/reference SST in both the ACSPO NLSST and Clear-Sky Mask algorithms ([15], [16], [17]). In NRT processing, the same day's L4 analysis is typically not available at the time of production and previous day's analysis is used. In contrast, during reprocessing, the same day's analysis SST is always available. Typically, the impact of using a day-old reference SST is minor, except in dynamic regions such as the Gulf Stream, where strong oceanic features such as thermal fronts can move significantly in 24 hours.
3. NRT data are validated in the NOAA SQUAM and ARMS systems at a latency of 3-4 days, which is enough to ensure the availability of most *in situ* data in *i*Quam [18]. However, some *in situ* data can take longer to arrive and *i*Quam quality control uses sliding temporal windows for outlier removal, which benefits from availability of the data to the right on the time scale. Recall that *i*Quam data are organized into monthly files, which are updated daily until a final version is released for a given month on the 5th of the following month (e.g., the January *i*Quam file is available on 5 February). The delayed ACSPO RAN data benefit from more complete and higher quality *in situ* data.
4. Additional manual quality control is performed on RAN data. Modern earth-viewing satellites and sensors are stable and quality flags are present in L1b files to screen out invalid and/or reduced quality radiance and navigation data. However, occasionally, reduced quality satellite data may not be properly flagged as such and can make its way into the final SST product. Occurrence of reduced quality SST data is typically identified in the SQUAM online system [9], where validation is performed with a 4-day latency. The affected SST data (normally a few granules) are inspected manually by the NOAA SST team, and degraded granules are removed from archived datasets and input L1b files are flagged to be omitted in future RAN efforts. The most common cause of manual removal of data are orbital adjustments such as inclination maneuvers (or black body warm-up cool-down exercises early in the NPP mission). As of this writing, there have been 10 inclination adjust maneuvers in the NPP mission since its launch in Oct'2011 and one during the N20 mission (launched in Nov'2017). For all these events, manual data removal was necessary. A list of in orbit events and anomalies for NPP, N20 and Metop missions can be found on the Integrated Calibration/Validation System (ICVS) Long-Term Monitoring online system [19].

Reanalysis efforts of both PM and AM SST products are currently underway at NOAA STAR. We estimate that reprocessing of both PM and AM SSTs will be complete and made available to users by summer 2021. Work is also underway with the Physical Oceanography Distributed Active Archive Center (PO.DAAC) to archive the L3S-LEO data.

This work is organized as follows. In section 2 we demonstrate recent improvements to the ACSPO L3S-LEO algorithm aimed at mitigation of cloud leakages and improving quality of SST imagery. In Section 3 we present results of consistency checks between L3S-LEO PM/AM against ACSPO GEO SST data, with emphasis on demonstrating the capability of the L3S-LEO SST products to capture the diurnal cycle. Section 4 contains conclusion and future plans for the ACSPO L3S suite of products.

2. ACSPO Collation Algorithm Improvements

2.1. Revised L3S SST reference

Recall that a central part of the ACSPO L3S-LEO algorithm is the debiasing of input L3U SST data to some reference SST, which is considered more accurate than a single satellite overpass [4]. This step is necessary to mitigate inter-overpass biases between consecutive overpasses from the same or different satellites. Inter-overpass biases can be attributed to the different viewing geometry, with atmospheric correction in the SST equations performed for different atmospheric paths [15]. They can also be attributed to different measurement times due to cloud movement or diurnal warming/cooling. If inter-overpass biases are not mitigated before combining data from multiple overpasses, discontinuities and/or stitching artifacts will be present in L3S imagery near swath edges as well as at the cloud boundaries [4]. In this work we refer to this SST reference as the "L3S reference" to avoid confusion with "first guess" or "reference" SST (typically an L4 analysis

SST product, such as CMC [14], OSTIA [20], GPB [21], MUR [22], RAMSSA [23] or Reynolds [24]) used in ACSPO SST and clear-sky mask algorithms ([15], [17]).

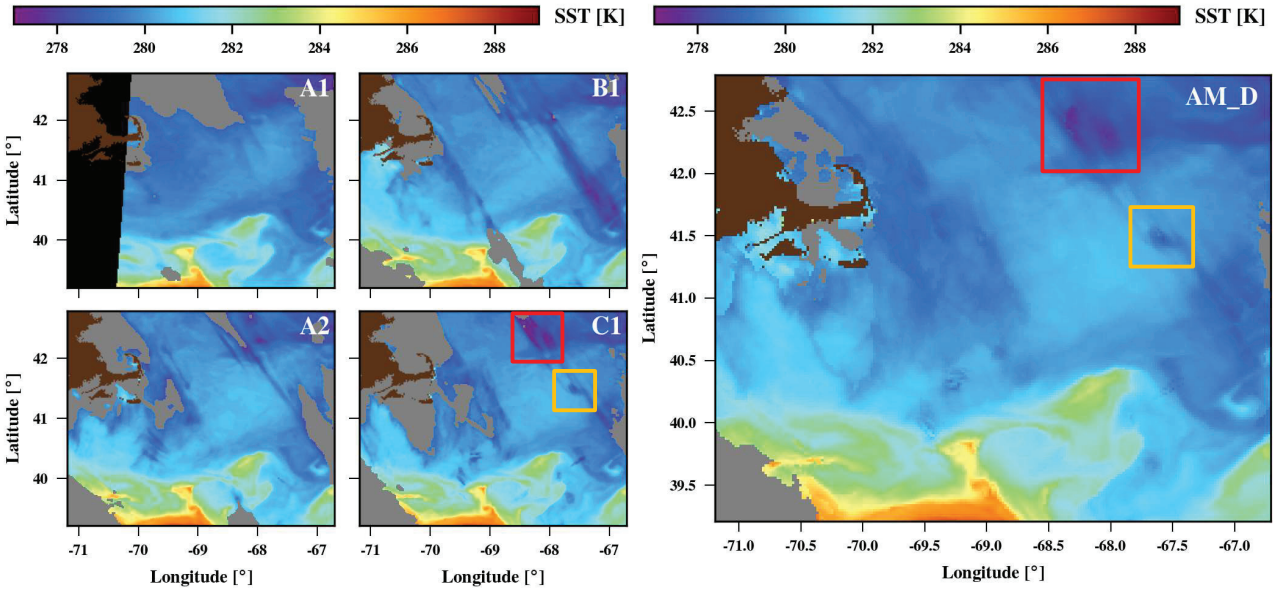

Figure 2. ACSPO subskin SST imagery from the North American East Coast (Georges Bank/Nantucket Shoals) on 29 Apr 2020. Left panels show L3U imagery from four overpasses labeled as A1 (Metop-A; 12:40 UTC), B1 (Metop-B; 14:00 UTC), A2 (Metop-A; 14:20 UTC) and C1 (Metop-C; 14:50 UTC). Right panel shows the corresponding L3S-AM SST imagery computed using the previous LVZA composite algorithm. Red and orange rectangles identify regions where cloud leakages have been propagated from the C1 overpass to the final L3S-AM SST product.

In early development version of the ACSPO L3S-LEO algorithm, the initial L3S reference used to debias individual sensor L3U overpasses was the lowest VZA (LVZA) composite, constructed by selecting in every 0.02° grid cell the SST measurement corresponding to the lowest VZA available during the 24-hour collation period. In previous work, we showed that this choice of L3S reference was effective at mitigating inter-overpass biases at both swath and cloud edges [4]. However, long term evaluation of L3S imagery in the ARMS online system [7] revealed that in some cases this approach leads to propagation of cloud leakages from L3U to L3S in case when the lowest VZA overpass was suboptimal, due to large scale (~10 pixel wide or more) cloud leakages, while smaller scale cloud leakages (speckly clouds) were adequately mitigated. As an example of shortcomings of LVZA compositing, the left panel of Fig. 2 shows ACSPO L3U daytime SST imagery from four Metop overpasses. The four overpasses are referred to as A1, B1, A2 and C1, with A/B/C referring to Metop-A/B/C and numbers refer to overpasses in chronological order (A1 is the Metop-A overpass preceding A2). The resulting super collated AM-D product, computed using the LVZA SST for the initial L3S reference, is also shown in the right panel of figure 2. The scene was chosen because it is particularly difficult for cloud masking, due to the presence of multiple clouds, for which the retrieved SST was only 1-3 K colder than surrounding clear sky. As a result, individual sensor L3U SST products contain small residual yet multiple cloud leakages. What made this scene particularly challenging for the collation was that the LVZA overpass (C1; average VZA of 26.6°) contained large cloud leakages, and the cleanest (least cloud leakages) overpass (A1) had the highest average VZA (64.9°). The B1 and A2 overpasses had intermediary average VZA of 46.0° and 47.7°, respectively. As a result, the LVZA L3S reference (shown in Fig. 3a) contains large scale cloud leakages and stitching artifacts, which are propagated into the final L3S product. Prominent cloud leakages in the C1 overpass and AM SST are marked by red and orange rectangles in Fig. 2.

To reduce impact of cloud leakages in low VZA overpasses on the L3S SST, we revised the procedure for computing the initial L3S reference SST. Instead of an LVZA composite we now use a weighted average with weights computed as

$$w_i \propto e^{-S_i/S_0} \times LCR_i^2, \quad (1)$$

where $S_i = \sec(\theta_i) - 1$, θ_i being the VZA, and the LCR_i is the ratio of clear sky pixels with respect to total number of ocean pixels in a local window at pixel indexed by *i,* and S_0 is a constant, which controls how strongly measurements with lower VZA are preferred (the LVZA composite is the limit as $S_0 \to 0$). The value of $S_0 = 1.33$ was empirically found to give a good balance between preference of lower VZA and higher LCR and is used in ACSPO V2.80.

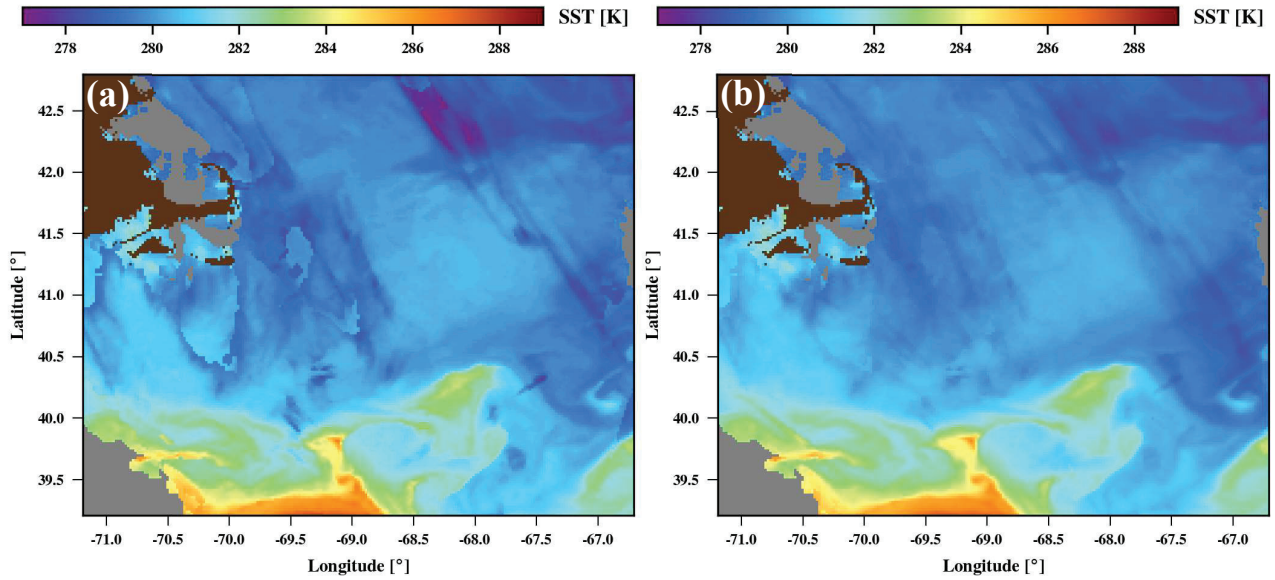

Figure 3. Initial L3S reference for the subskin SST imagery from the same date and location as in Fig. 2. (a) LVZA SST (lowest VZA composite). (b) LVW SST (LCR-VZA weighted) using weights computed using Eq. (1).

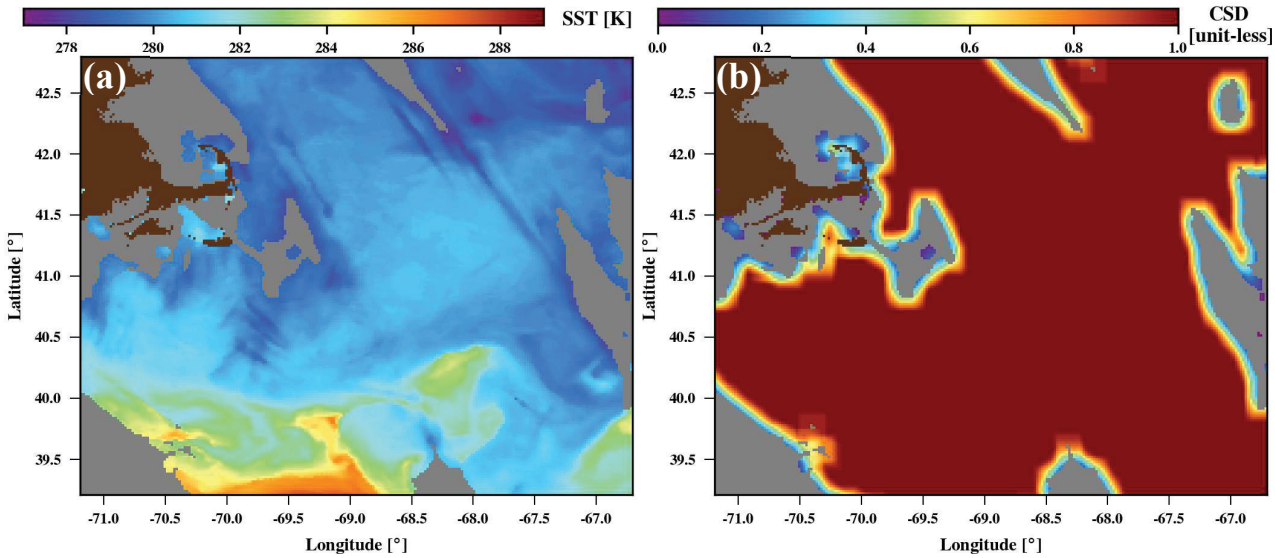

Figure 4. (a) Subskin SST from A2 overpass (see Fig. 2 captions for more details). (b) Local clear-sky ratio (LCR) corresponding to SST in (a).

The local clear-sky ratio (LCR) is defined as a mean within an 11×11 pixel sliding window (centered at pixel *i*) of a matrix whose elements are 1 for clear-sky and 0 for cloudy conditions. This means that $LCR_i \in [0,1]$, with $LCR_i \simeq 1$ in large contiguous regions of clear sky, $LCR_i \simeq 0.5$ at cloud boundaries and $LCR_i \simeq 0$ in small patches of clear sky. We will refer to SST calculated using weights from Eq. (1) as LCR-VZA weighted (LVW) SST. The idea is that measurements made at

lower VZA and far from clouds (in regions of high LCR) get assigned the highest weight. Our motivation is that we want to take advantage of the higher accuracy and spatial resolution of SST retrievals at low VZA while also placing lower weight on SST measurements at cloud boundaries and small patches of clear sky. This choice of weighting scheme is based on our observation from the ARMS [7], consistent with intuition, that SST measurements from regions of bulk clear sky are typically more reliable (fewer cloud leakages) than measurements from regions with scattered clouds or near cloud boundaries. Figure 4 shows SST imagery from the A2 overpass (panel a) and corresponding LCR (panel b), demonstrating how pixels in isolated patches of clear-sky and cloud boundaries get assigned lower weight. The A2 overpass was chosen as a demonstrative example due to the presence of many cloud boundaries as well as small, isolated patches of clear sky.

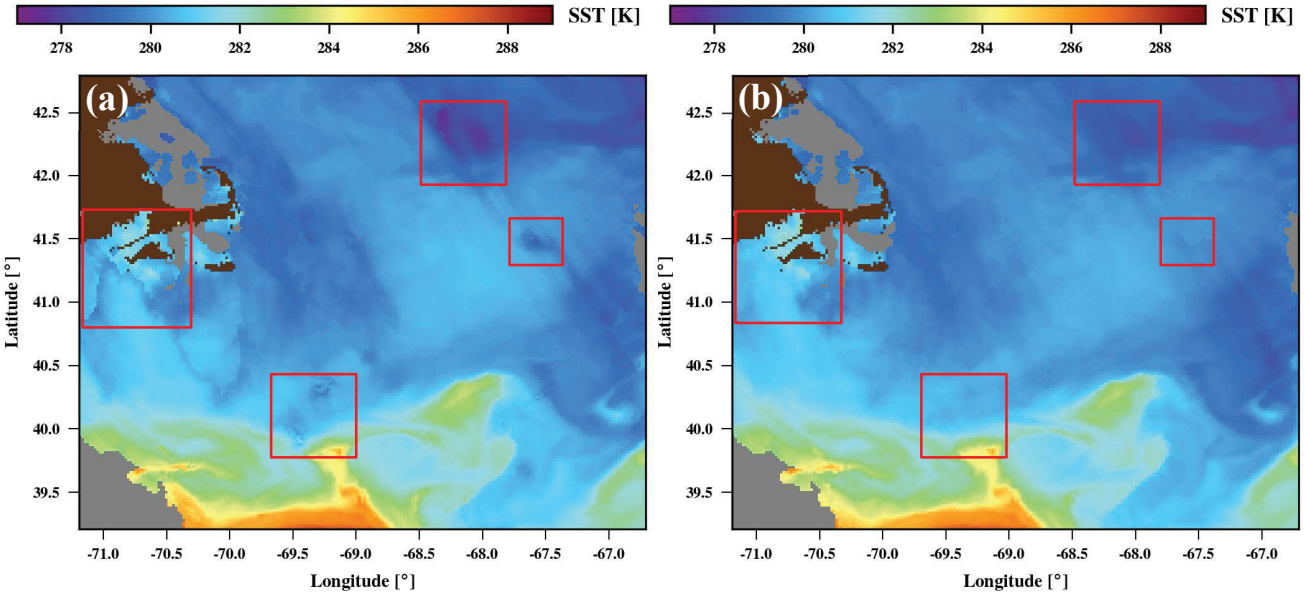

Figure 5. Daytime L3S-AM subskin SST imagery computed using (a) LVZA and (b) LVW SST (shown in Figure 3) as initial L3S reference. Red rectangles highlight areas that are substantially improved when LVW SST is used.

Figure 3 shows comparison of LVZA and LVW L3S reference SSTs from the same scene as in Figs. 2-3. While the cloud leakages and stitching artifacts are still present in the LVW SST, they are much less prominent compared to those in the LVZA SST. Figure 5 shows a comparison of the resulting L3S SST when using LVZA (a) and LVW (b) SST as an initial L3S reference. We can see that in both cases the L3S SST is substantially improved, compared to their respective L3S references in Fig. 3 (either LVZA or LVW). However, the L3S SST using LVZA as L3S reference contains multiple residual cloud leakages and discontinuities (denoted by red rectangles in Fig. 5) that are propagated into the L3S (although reduced in magnitude) from the LVZA SST. Although not perfect, the L3S SST using the LVW initial reference is a substantial improvement. Figure 6 shows a similar comparison of LVZA vs. LVW reference SST as in Fig. 4, but for a different scene over the Monterey Bay on the US west coast, using SST data from the PM-D SST product, produced from two VIIRS instruments flown onboard NPP and N20. Figure 6 shows that both the LVZA and LVW SSTs contain multiple residual cloud leakages and stitching artifacts. However, in the case of LVW, imagery artifacts are reduced to a point where the ACSPO L3S-LEO adaptive weighting algorithm is capable of mitigating shortcomings in the LVW SST L3S reference. This is demonstrated in Fig. 7, which shows the resulting L3S SST when LVZA and LVW SSTs are used as the initial references. In both cases, the resulting L3S SST is significantly improved compared to the initial L3S reference. However, the L3S SST produced using the LVW SST, had a better initial reference which results in superior SST image quality.

In Figs. 2-7, daytime L3S-LEO products (AM-D and PM-D) were used for demonstration of ACSPO L3S algorithm improvements. The reason for this choice is that the daytime ACSPO L3U SST products typically exhibit greater inter-overpass biases than their nighttime counterparts and are therefore better suited for demonstration purposes. The reason for this is two-fold. Firstly, the day-time SST retrievals are less accurate than nighttime due to the absence of the atmospherically transparent mid-infrared 3.7 μm channel (channel M12 for VIIRS and 3B for AVHRR-3), which cannot be used during daytime for SST retrievals due to contribution by reflected solar radiation [15]. Secondly, during daytime there can be real inter-overpass biases due to diurnal warming/cooling, which is complicated even further by subskin-depth

SST differences during strong diurnal warming events. Inter-overpass bias due to diurnal warming/cooling is more of a concern for the PM-D SST than for other three L3S-LEO products, because it has the strongest diurnal warming, as will be shown in section 3.

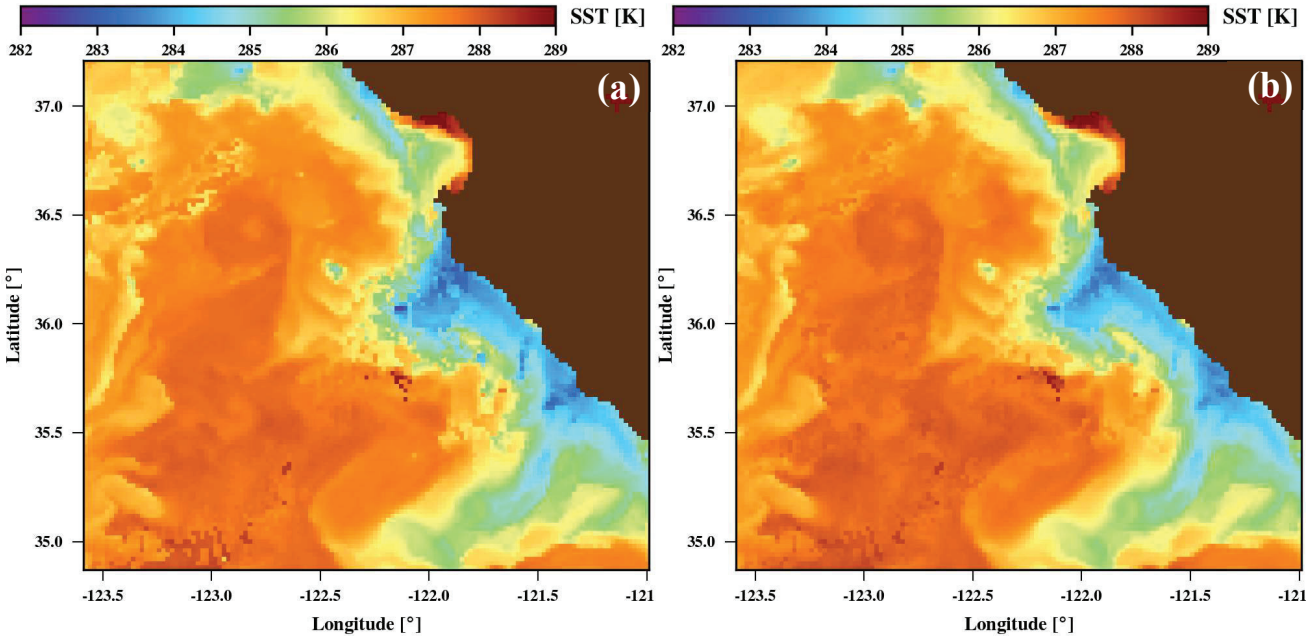

Figure 6. Daytime L3S-PM initial reference subskin SST imagery from the US West Coast (Monterey Bay; 30 Apr 2020). (a) LVZA (lowest VZA composite) SST. (b) LVW (LCR-VZA weighted) SST using weights computed using Eq. (1).

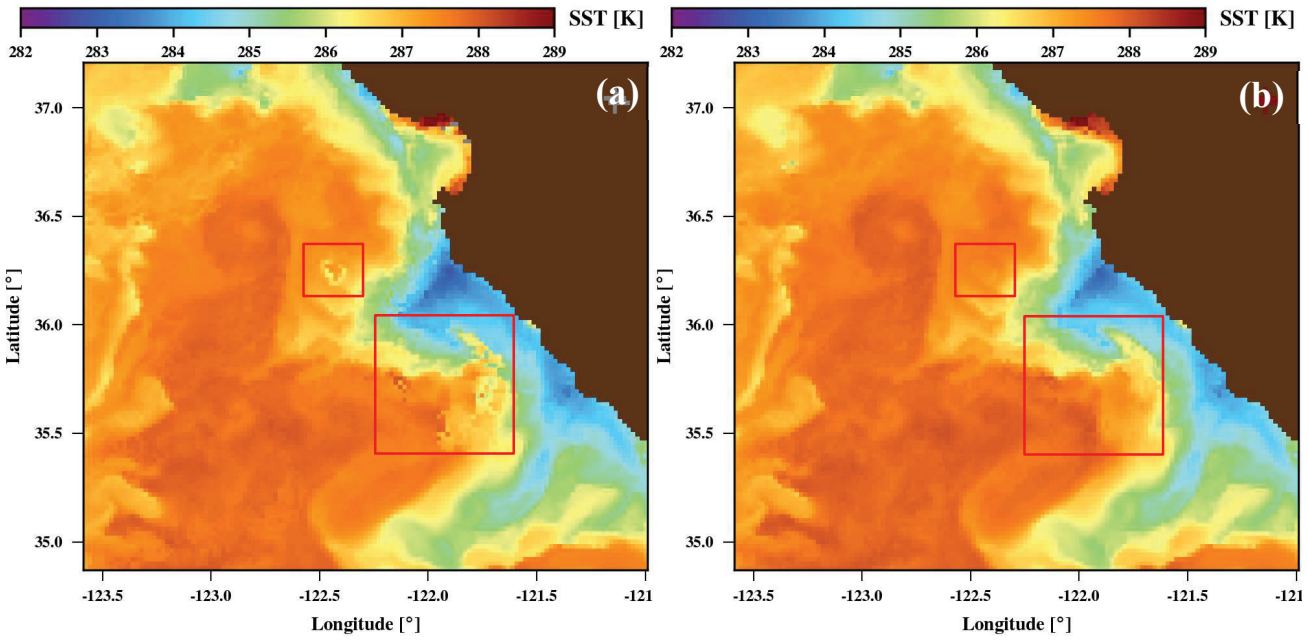

Figure 7. Daytime L3S-PM subskin SST imagery from US West Coast (Monterey Bay; 30 Apr 2020) using LVZA SST (a) and LVW SST (b) for initial L3S reference. Red rectangles highlight areas that are substantially improved when LVW SST is used.

2.2 Iterative Debiasing

The second improvement to the ACSPO L3S-LEO original algorithm [4] is that the inter-overpass debiasing of L3U input data is now performed iteratively, with the L3S SST from a previous iteration used as an L3S reference instead of the LVW SST, which is only used in the first iteration. In our earlier work [4], the input L3U data were only debiased once using the LVZA SST as a L3S reference. We will refer to these iterations as 'debiasing iterations', to distinguish it from another iterative scheme employed in the ACSPO L3S-LEO adaptive weighting algorithm [4]. While the LVW initial reference described earlier in this section is superior to the LVZA reference, it may still have artifacts that can be mitigated using an adaptive weighting scheme. In most cases, the resulting improvement from further debiasing iterations is relatively minor and may not as clearly visible on the length scales and dynamic SST ranges present in the scenes in Figs. 5 and 7. However, as will be shown later, in extreme cases (typically close to strong thermal fronts or near regions with extreme inter-overpass bias), the benefits of further debiasing iterations may be seen in up to three iterations (two additional iterations after using the LVW SST as the initial L3S reference).

In the revised ACSPO L3S algorithm, debiasing iterations use progressively smaller debiasing windows, which allow progressively smaller scale deviations from the L3S reference. The first LVW iteration uses a 21×21 window, which was chosen to be large enough to mitigate regional inter-overpass biases. However, this window may be comparable to the typical sizes of thermal fronts. As a result, the debiasing procedure can reduce the strength of thermal fronts (its cold side gets warmer, and the warmer side gets colder), especially in multiple iterations. This effect is difficult to notice on a 2D color plot, but clearly apparent when plotting the SST profile along 1D constant latitude/longitude transactions. To demonstrate this point, Fig. 8 shows daytime L3S-AM SST in a dynamic region (Agulhas Current) and Fig. 9 shows two SST curves along the two paths, corresponding to a constant latitude (marked by the horizontal black lines) and constant longitude (marked by the vertical black lines) in Fig. 8. The constant-latitude path intersects a strong thermal front with a temperature difference of 3.5 K between the warm and cold sides. The SST along the constant latitude path is shown in Fig. 9b. Figure 9b shows that SST gradient in the first iteration is reduced compared to iterations 2 and 3, which use a debiasing window of 11×11 and 7×7, respectively. Another benefit of multiple debiasing iterations is mitigation of discontinuities in the L3S SST imagery. An example of SST discontinuity mitigation is also shown in Fig. 8. Black arrows denote unphysical discontinuities in SST imagery that are reduced in the second iteration and are not visible after the third iteration. To better visualize the changes, Fig. 9a shows SST from the same scene along a constant longitude path (denoted by black vertical line). The path intersects an SST discontinuity which is denoted by black arrows in Figs. 8 and 9a. Figure 9a demonstrates how the discontinuity in SST imagery is mitigated by further debiasing iterations.

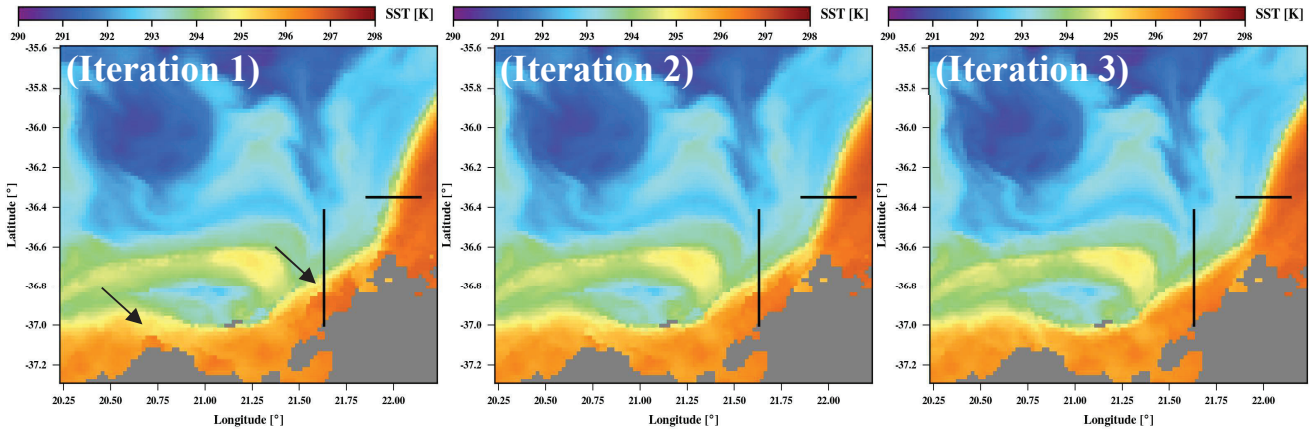

Figure 8. Daytime ACSPO L3S-AM subskin SST imagery from the Agulhas Current on 29 Apr 2020. The three panels show L3S SST after the 1st, 2nd and 3rd debiasing iterations (from left to right). Black lines denote paths of constant longitude and latitude, along which the 1D plots of SST are shown in Figs. 9a and 9b, respectively, to better illustrate the improvement in SST imagery with additional debiasing iterations. Black arrows in left panel point to discontinuities in L3S SST imagery computed using only one debiasing iteration.

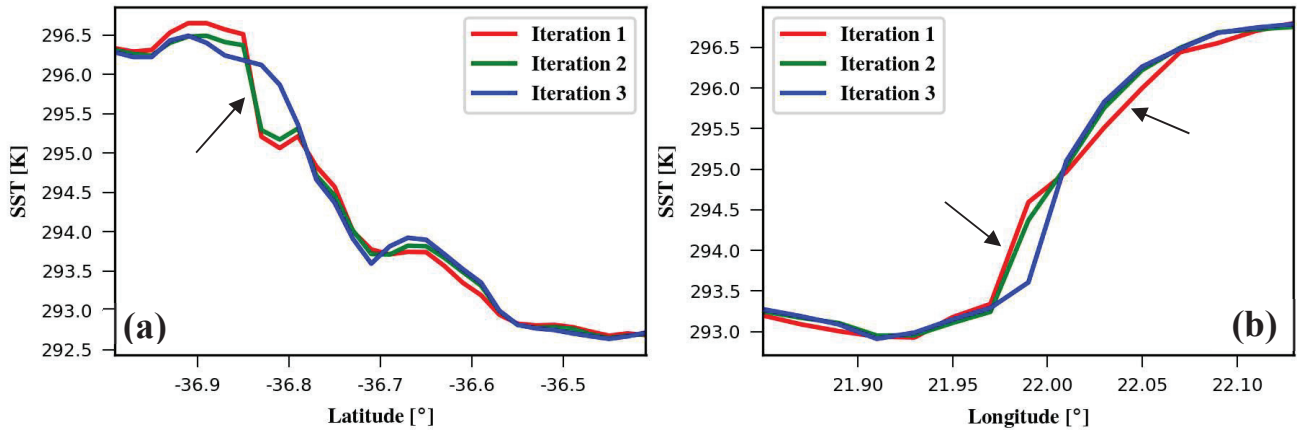

Figure 9. One dimensional L3S-AM SST profiles from the scene shown in Figure 8. (a) Subskin SST along the constant longitude path denoted by the black vertical line in Fig. 8. Arrow denotes discontinuity in SST that is mitigated by further debiasing iterations. (b) Subskin SST along the constant latitude slice denoted by the black horizontal line in Fig. 8. The constant latitude slice passes through a strong front that is reduced in magnitude (denoted by arrows) when only one or two debiasing iteration are performed.

3. Initial look at the diurnal cycle in L3S-LEO vs GEO SST

ACSPO L3S-LEO PM/AM products are reported twice daily (day and night), sampling the SST diurnal cycle at four local solar times, approximately centered at 01:30 (PM; night), 09:30 (AM; day), 13:30 (PM; day) and 21:30 (AM; night). In this section we show that further aggregation in time would reduce the L3S-LEO's capability to resolve the diurnal cycle. Figure 1 shows normalized number of observations as a function of local time for all four L3S-LEO products based on monthly aggregated data from January 2020. Figure 1 shows that the spread of local solar time observation is about 2 hours and there is minimal overlap between the four SST products. Figure 10 shows an example diurnal cycle of *in situ* SST minus foundation SST; stratified by the local solar time). Colored overlay show approximate temporal coverage of the different L3S-LEO products. The centers of the colored rectangles approximately correspond to each product's local equator crossing times (for example 01:30am for the PM-N) and the width is the approximate 2-hour full width at half maximum (FWHM) of corresponding peaks in histogram shown in Fig. 1. Figure 10 shows that the PM-D SST should capture the near-peak of the diurnal cycle and is therefore essential to estimate the diurnal cycle amplitude. The PM-N SST is a close proxy for the foundation SST with the AM-D SSTs being close to the PM-N, with the diurnal warming ~0.01 K stronger on average and more variable (magnitude of derivative of diurnal warming with respect to local time is greater for the AM-D than the PM-N). The AM-N observes intermediary diurnal warming between those for the AM-D and PM-D. Note that Fig. 10 only shows the potential of ACSPO L3S-LEO products to capture the diurnal cycle based on local time of observations. In this section we will demonstrate this capability, by comparing the L3S-LEO satellite SST diurnal cycle to that of ACSPO SST from the ABI instrument flown onboard the GOES-16 (G16) geostationary satellite.

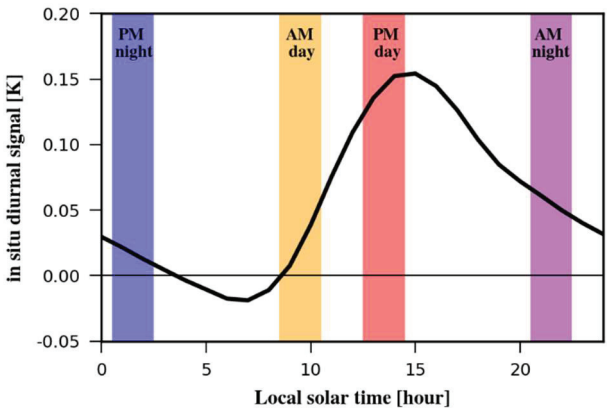

Figure 10. Diurnal cycle in *i*Quam *in situ* SSTs from drifters and tropical moorings from January 2020. CMC L4 foundation SST was subtracted to normalize the data. Colored rectangles denote approximate temporal coverage of all four L3S-LEO SST products. The center of each rectangle is the local crossing time of the corresponding platforms and the width is 2 hours, which is the approximate FWHM of the corresponding peaks in the histograms shown in Fig. 1.

Recall that SST reported in ACSPO files as "sea_surface_temperature" (produced with the "global regression" SST, GR SST), is a proxy for subskin SST. Global regression means that a single set of regression coefficients are used for SST retrievals (only stratified by day and night). ACSPO files also report the 'SSES bias', which is an estimate of bias with respect to *in situ* data. The ACSPO SSES algorithm is based on a piece-wise regression (PWR), where separate set of coefficients are derived using stratification in regressors' space [16]. Subtracting the SSES bias from the subskin SST results in SST that is a better proxy for *in situ* SST at a depth of approximately 0.2-1.0 m and is therefore referred to in ACSPO as 'depth SST'. Note that regression coefficients for the GR and PWR algorithms are trained against *in situ* data, and are unique to each sensor/satellite ([12], [16]).

The ACSPO L3S-LEO temporal resolution (four points every 24 hours) is degraded compared to the modern geostationary (GEO) sensors such as ABI flown onboard GOES-16/17 and AHI onboard Himawari-8/9, which both report full disc images every 10 minutes and hourly collated-in-time ACSPO SST products are available for all three platforms ([25], [26], [27]). However, sensors onboard the LEO platforms such as NPP, N20 and Metop-FG have the advantage of providing global coverage including much more compete coverage of high latitudes, which are viewed under unfavorable conditions by geostationary sensors. The L3S-LEO family of products can be thus an invaluable addition to GEO SST for studying the global SST diurnal cycle.

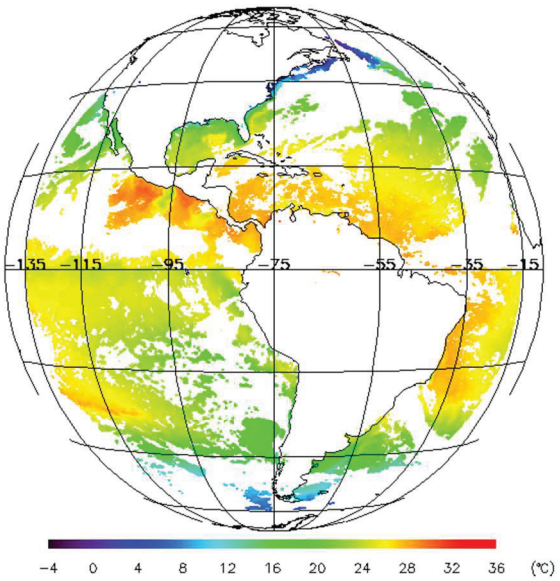

Figure 11. ACSPO V2.70 G16 L3C subskin SST on 19 Jan 2021 at 00:00Z. SST is reported for all ice-free pixels over water where satellite zenith angle is 67° or smaller.

In this study, we preliminarily compare ACSPO L3S-LEO subskin and depth SSTs to those of G16 for one full day of 19 Jan 2021. Figure 11 shows an example full disc G16 SST imagery for the day in question at 00:00Z. The ACSPO G16 L3C SST product is reported every hour (UTC; 24 files/day). Only those 0.02° L3 grids were used here in which (a) all 4 L3S-LEO points, and (b) at least 22 (out of 24) hourly (UTC) GEO SSTs were available. This resulted in approximately 1.4 million diurnal cycles being compared. We define ΔSST as the difference between the satellite SSTs and foundation CMC L4 SST [11]. For this comparison UTC time was converted to local time (LT) and the resulting ΔSST were binned based on the LT with a bin size of 1 hour. All GEO ΔSSTs within each hourly LT bin were then averaged. L3S-LEO SST retrieval time was also converted to LT and all 1.4M points averaged (both ΔSSTs and the LTs).

Figure 12 shows results of comparison of G16 and L3S-LEO subskin SST diurnal cycle. Subskin G16 SST (solid blue curve) shows a pronounced diurnal cycle, reaching a minimum around 5am and maximum around 3-4pm, with an amplitude of ~0.59 K. The L3S-LEO diurnal cycle largely follows GEO, but is offset by ~-0.09 K. The dashed red curve shows the G16 diurnal cycle shifted downward by 0.09 K to minimize difference with respect to the four L3S-LEO data points (red circles). The minimum ΔSSTs of both G16 and LEO diurnal cycles are expected to be close to 0 K (foundation SST), but in fact they bracket 0 K by about ±0.04 K. Figure 13 shows the corresponding depth SST diurnal results. The G16 depth SST in Fig. 13 shows a clear diurnal cycle, reaching a minimum between 5-6am and maximum around 3pm local time. The amplitude of the diurnal cycle in the G16 depth SST is ~0.45 K, which is smaller (as expected) than for the subskin (0.59 K). As in the case for subskin SST, the L3S-LEO diurnal cycle largely follows that of G16, but is offset by ~-0.07 K, which is slightly smaller compared to the offset in the subskin SST (~-0.09 K). The minimum of the depth ΔSSTs diurnal cycles is comparable to subskin and bracket 0 K by ±0.03 K.

In summary, our preliminary and limited analyses analyses of the diurnal cycle in the subskin and depth SSTs in Figs. 12 and 13 show that GEO and L3S-LEO diurnal cycles are qualitatively and even quantitatively consistent, for an arbitrarily selected day of 19 January 2021, although offset by 0.07-0.09K. This consistency is encouraging, as all LEO SSTs are derived using different algorithms during day and night, and each separately trained against *in situ* SSTs. We note that agreement of the average GEO and L3S-LEO diurnal cycles is a necessary condition for their consistency, but may not be sufficient. More in-depth analyses are underway to ensure better quantitative agreement on average, and more regional and local checks.

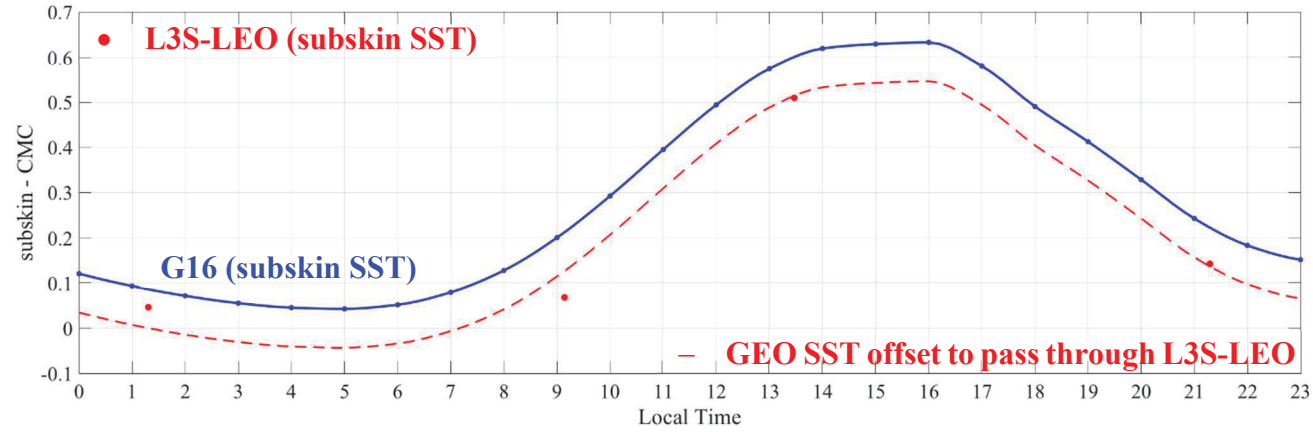

Figure 12. ΔSST = Satellite – foundation SST stratified by local solar time with a bin size of 1 hour. Solid blue curve shows the G16 subskin diurnal cycle and red dots denote results for all four L3S-LEO SSTs. Dashed red curve shows the G16 diurnal cycle shifted downward by 0.09 K to minimize difference with respect to the four L3S-LEO data points. Both G16 and LEO SST data are from 19 Jan 2021.

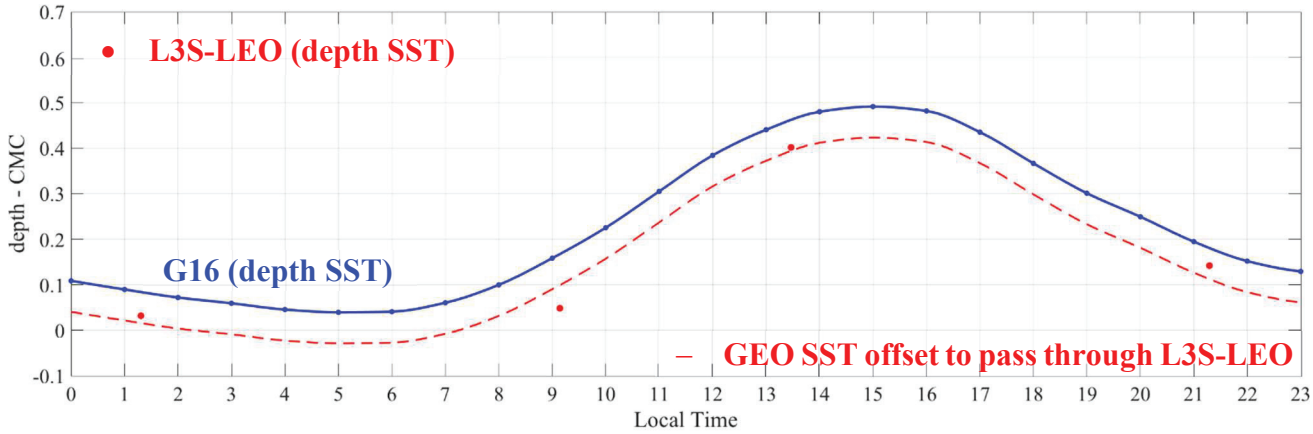

Figure 13. Same as in Fig. 12 but for depth SST. Dashed red curve shows the G16 diurnal cycle shifted downward by 0.07 K.

4. Conclusion and Future Work

We described recent updates to the ACSPO L3S-LEO algorithm for collation of L3U SSTs from the high-resolution earth viewing sensors VIIRS and AVHRR FRAC, flown onboard LEO platforms NPP/N20 and Metop-A/B/C, respectively. Two algorithmic updates were proposed and demonstrated to improve the quality of SST imagery, and to mitigate cloud leakages present in individual sensor L3U data:

1. The initial L3S-based reference used to debias/normalize input L3U data was revised. Previously we used a lowest VZA composite containing the SST measurement made at the lowest VZA (LVZA) available during the 24-hour collation period [4]. In this work we showed that this choice of L3S reference can lead to propagation of residual cloud leakages and imagery discontinuities to the L3S SST. We proposed and demonstrated an improved scheme where the L3S reference is constructed by weighting L3U SST based on both VZA and local clear-sky ratio (LCR). We call this L3S reference the LCR -VZA weighted (LVW) SST.
2. In a previous version of the ACSPO L3S-LEO algorithm, mitigation of inter-overpass biases by debiasing/normalizing of input L3U data was only performed once using the LVZA L3S reference [4]. In this work we proposed and demonstrated an improved algorithm, where input L3U is debiased multiple times in an iterative manner. The first debiasing iteration is performed using the LVW SST and in later iterations the

L3S SST from the previous iteration is used instead of the LVW SST. Further iterations more aggressively debias/normalize L3U input to the L3S reference, converging on the final L3S SST after three iterations. We showed that this approach leads to reduced smoothing of sharp SST features as well as mitigation of discontinuities in L3S SST imagery.

One of the major motivations for segregating L3S-LEO products into four files per day (PM and AM; day and night) is that further merging would result in the loss of L3S-LEO's capability to resolve the diurnal cycle. In this work we demonstrated the capability of ACSPO L3S-LEO SST to resolve the diurnal cycle by comparing L3S-LEO satellite SST diurnal cycle to that of ACSPO SST from the ABI instrument flown onboard the GOES-16 (G16) geostationary satellite. We found that the L3S-LEO and G16 diurnal cycles are in qualitative and even quantitative agreement, for both subskin and depth SSTs, for one randomly chosen day. This result is promising, since all LEO SSTs are derived using different algorithms during day and night, and each separately trained against *in situ* SSTs. However, more detailed analyses are necessary to ensure better quantitative agreement over longer time periods and regions outside the view of G16 ABI.

Many users of ACSPO SST products have expressed interest in a daily aggregated L3S-LEO product. In response, the NOAA SST team is investigating feasibility of a L3S-LEO product which combines the PM and AM, both daytime and nighttime SSTs, into a single daily SST product. As we have shown in this work, each L3S-LEO product samples a subset of the diurnal cycle, so care must be taking when merging different L3S-LEO products. Such a daily product will likely result in a lower feature resolution, where significant movement of ocean features (compared to the L3S 0.02° grid) takes place over the course of a day.

Future ACSPO L3S-LEO development will focus on adding more sensors to the AM and PM L3S-LEO lines, which currently only includes two VIIRSs onboard NPP/N20 and three AVHRR FRACs onboard the Metop-FG constellation (Metop-A/B/C). Plans for inclusion of more sensors into the ACSPO L3S-LEO line include:

- Once launched, N21 VIIRS will be added to the PM-line.
- METimage will be flown onboard Metop-SG constellation of satellites (estimated launch in 2023), which is the successor of the current Metop-FG constellation. Metop-SG satellites will fly in the same mid-morning AM orbit as its Metop-FG predecessors. We will explore including it in the ACSPO L3S-LEO AM line.
- Depending upon users' interest and available development resources, we will consider extending the high-resolution L3S-LEO PM SST time series (Feb'2012 – on) and AM (Dec'2006 – on), by adding Aqua MODIS (launched in 2002) to the PM line and Terra MODIS (launched in 2000) to the AM line. Note that the Terra equator crossing time of 10:30 is shifted by an hour compared to Metop-FG (9:30), which may require special treatment of Terra to seamlessly extend the AM time series before Metop-A SST data availability (2006).
- Before MODIS Terra/Aqua time frame, the high resolution L3S-LEO SST products may be supplemented from the AVHRR GAC instruments flown onboard numerous NOAA satellites starting with NOAA-7 (launched in 1981). Their L3 grid is the same as from hi-res sensors (0.02°), but effective feature resolution is lower. Also their orbits have not been controlled, unlike the hi-res sensors MODIS, AVHRR FRAC and VIIRS.

In addition to the ACSPO L3S-LEO family, an L3S-GEO family of SST product is currently in development at NOAA [28].The L3S-GEO family will contain hourly super-collated SST data from the current generation of earth-viewing geostationary platforms such as the GOES-R series (GOES-16/17; carrying ABI), Himawari (Himawari-8/9; carrying AHI) as well as future GOES-T/18 also carrying the ABI, and Meteosat Third Generation carrying the Flexible Combined Imager (FCI) sensors. Our ultimate goal is to finally combine the L3S-LEO and L3S-GEO families into one single ACSPO L3S SST product, with global coverage (advantage of LEO) and 1hr temporal resolution (advantage of GEO).

Acknowledgement

This work is supported by the Joint Polar Satellite System (JPSS) Program (Mitch Goldberg, JPSS Program Scientist; Lihang Zhou, JPSS Program Manager; Alisa Yong, JPSS STAR Manager). The views, opinions, and findings in this report are those of the authors and should not be construed as an official NOAA or U.S. government position or policy.

References

[1] GHRSST Science Team, "The Recommended GHRSST Data Specification (GDS) 2.0, document revision 5," 2012. [Online]. Available: https://www.ghrsst.org/wp-content/uploads/2016/10/GDS20r5.pdf.

[2] A. Ignatov, I. Gladkova, Y. D. Ding, F. Shahriar, Y. Kihai and X. Zhou, "JPSS VIIRS level 3 uncollated sea surface temperature product at NOAA," *Journal of Applied Remote Sensing,* vol. 3, pp. 1-17, 2017.

[3] I. Gladkova, M. Pennybacker, A. Ignatov and Y. Kihai, "Towards high-resolution multi-sensor gridded ACSPO SST product: reducing residual cloud contamination," *SPIE,* vol. 11014, pp. 138-149, 2019.

[4] O. Jonasson, I. Gladkova, A. Ignatov and Y. Kihai, "Progress with development of global gridded super-collated SST products from low Earth orbiting satellites (L3S-LEO) at NOAA," *SPIE,* vol. 11420, pp. 5-22, 2020.

[5] O. Jonasson and A. Ignatov, "Status of second VIIRS reanalysis (RAN2)," *SPIE,* vol. 11014, pp. 150-156, 2019.

[6] V. Pryamitsyn, B. Petrenko, I. A., O. Jonasson and Y. Kihai, "Historical and near-real time SST retrievals from Metop AVHRR FRAC with the advanced clear-sky processor for ocean," *SPIE,* vol. 11752, pp. 1-16, 2021.

[7] Y. Ding, A. Ignatov, K. He and I. Gladkova, *ACSPO Regional Monitor for SST (ARMS) v2.10,* GHRSST, available at ftp://ftp.star.nesdis.noaa.gov/pub/sod/osb/aignatov/GHRSST/G19/Presentations, 2010.

[8] NOAA CoastWatch, "CoastWatch ACSPO L3S-LEO," [Online]. Available: https://coastwatch.noaa.gov/cw/satellite-data-products/sea-surface-temperature/noaa-acspo/l3s-leo.html. [Accessed 27 January 2021].

[9] P. Dash, A. Ignatov, Y. Kihai and J. Sapper, "The SST Quality Monitor (SQUAM)," *JTECH,* vol. 27, pp. 1899-1917, 2010.

[10] Q. Liu, P. van Delst, Y. Chen, D. Groff, Y. Han, A. Collard, F. Weng, S.-A. Boukabara and J. Derber, "Community radiative transfer model for radiance assimilation and applications," in *IEEE International Geoscience and Remote Sensing Symposium*, Munich, Germany, 2012.

[11] Joint Center for Satellite Data Assimilation, "Community Radiative Transfer Model (CRTM) wiki," [Online]. Available: https://github.com/JCSDA/crtm/wiki. [Accessed 25 1 2021].

[12] NOAA National Centers for Environmental Prediction (NCEP), "NOAA/NCEP Global Forecast System (GFS) Atmospheric Model," 2011. [Online]. Available: https://www.emc.ncep.noaa.gov/emc/pages/numerical_forecast_systems/gfs. [Accessed 25 1 2021].

[13] M. M. Rienecker, M. J. Suarez, R. Gelaro, R. Todling, J. Bacmeister, E. Liu, M. G. Bosilovich, S. D. Schubert, L. Takacs, G.-K. Kim, S. Bloom, J. Chen, D. Collins, A. Conaty, A. d. Silva, W. Gu, J. Joiner, R. D. Koster, R. Lucchesi, A. Molod, T. Owens, S. Pawson, P. Pegion, C. R. Redder, R. Reichle, F. R. Robertson, A. G. Ruddick, M. Sienkiewicz and J. Woollen, "MERRA: NASA's Modern-Era Retrospective Analysis for Research and Applications," *J. Climate,* vol. 24, pp. 3624-3648, 2011.

[14] Canada Meteorological Center, *GHRSST Level 4 CMC0.1deg Global Foundation Sea Surface Temperature Analysis (GDS version 2),* CA: PO.DAAC, 2016.

[15] B. Petrenko, A. Ignatov, Y. Kihai, J. Stroup and P. Dash, "Evaluation and selection of SST regression algorithms for JPSS VIIRS," *JGR,* vol. 119, pp. 4580-4599, 2014.

[16] B. Petrenko, A. Ignatov, Y. Kihai and P. Dash, "Sensor-Specific Error Statistics for SST in the Advanced Clear-Sky Processor for Oceans," *JTECH,* vol. 33, p. 345–359, 2016.

[17] B. Petrenko, A. Ignatov, Y. Kihai and A. K. Heidinger, "Clear-sky mask for the advanced clear-sky processor for oceans," *JTECH,* vol. 27, pp. 1609-1623, 2010.

[18] F. Xu and A. Ignatov, "In situ SST Quality Monitor (iQuam)," *JTECH,* vol. 31, pp. 164-180, 2014.

[19] STAR, "Integrated Calibration/Validation System Long-Term monitoring," [Online]. Available: https://www.star.nesdis.noaa.gov/icvs/. [Accessed 27 April 2021].

[20] J. C. Donlon, M. Martin, J. Stark, J. Roberts-Jones, E. Fiedler and W. Wimmer, "The Operational Sea Surface Temperature and Sea Ice Analysis (OSTIA) system," *Remote Sensing of Environment,* vol. 116, pp. 140-158, 2012.

[21] E. Maturi, A. Harris, J. Mittaz, J. Sapper, G. Wick, X. Zhu, P. Dash and P. Koner, "A New High-Resolution Sea Surface Temperature Blended Analysis," *Bulletin of the American Meteorological Society,* vol. 98, no. 5, pp. 1015-1026, 2017.

[22] T. M. Chin, J. Vazquez-Cuervo and E. M. Armstrong, "A multi-scale high-resolution analysis of global sea surface temperature," *Remote Sensing of Environment,* vol. 200, pp. 154-169, 2017.

[23] H. Begs, A. Zhong, G. Warren, O. Alves, G. Brassington and T. Pugh, "RAMSSA - An Operational, High-Resolution, Multi-Sensor Sea Surface Temperature Analysis over the Australian Region," *Australian Meteorological and Oceanographic Journal,* vol. 61, pp. 1-22, 2011.

[24] R. W. Reynolds, T. M. Smith, C. Liu, D. B. Chelton, K. S. Casey and M. G. Schlax, "Daily High-Resolution-Blended Analyses for Sea Surface Temperature," *Journal of Climate,* vol. 20, no. 22, pp. 5473-5496, 2007.

[25] NOAA Center For Satellite Applications And Research (STAR), *GHRSST NOAA/STAR GOES-16 ABI L3C Western Atlantic SSTskin v2.70 dataset in GDS2,* Camp Springs: NASA Physical Oceanography DAAC, 2019.

[26] NOAA Center For Satellite Applications And Research (STAR), *GHRSST NOAA/STAR GOES-17 ABI L3C America Region SST v2.71 dataset in GDS2,* NASA Physical Oceanography DAAC, 2020.

[27] NOAA Center For Satellite Applications And Research (STAR), *GHRSST NOAA/STAR Himawari-08 AHI L3C Pacific Ocean Region SST v2.70 dataset in GDS2,* NASA Physical Oceanography DAAC, 2020.

[28] L. Hunger, A. Ignatov, I. Gladkova, Y. Kihai and O. Jonasson, "Towards super-collated gridded ACSPO SST product from multiple geostationary satellites (L3S-GEO)," *SPIE,* vol. 11752, 2021.